Deep-Sea Research I 110 (2016) 65–74

Contents lists available at ScienceDirect

Deep-Sea Research I

journal homepage: www.elsevier.com/locate/dsri

Deepwater overflow observed by three bottom-anchored moorings in the Bashi Channel

Xiaolong Zhao [a], Chun Zhou [a], Wei Zhao [a,*], Jiwei Tian [a], Xiaobiao Xu [b]

[a] Physical Oceanography Laboratory/Qingdao Collaborative Innovation Center of Marine Science and Technology, Ocean University of China, Qingdao, China
[b] Center for Ocean-Atmospheric Prediction Studies (COAPS), Florida State University, Tallahassee, FL, USA

ARTICLE INFO

Article history:
Received 23 March 2015
Received in revised form
5 January 2016
Accepted 5 January 2016

Keywords:
Deepwater overflow
Bashi Channel
Volume transport
Spatial structure
Temporal variability

ABSTRACT

Three moorings equipped with 10 current meters and 7 CTDs were deployed in the Bashi Channel, the main deep connection between the northwestern Pacific Ocean and the South China Sea, from August 2010 to April 2011 to investigate the deepwater overflow of the North Pacific Deep Water through it. Results from these observations provide, for the first time, valuable information on the spatial structure of the deep current and allow us to estimate the overflow transport with greater accuracy. The observed current is coherent both vertically and horizontally but exhibits a much stronger velocity in the central area compared to near the edges of the channel. The core of the overflow is found near 2600 m, with mean velocity, potential temperature, and salinity of 22.5 cm s^{-1}, 1.79 °C, and 34.64 psu, respectively. The current is approximately geostrophic, with isopycnals sloping upward to the right-hand side of the flow. The local Froude number is found much less than 1, implying that the deep flow in the Bashi Channel could not be hydraulically controlled. The observations yield an 8-month mean transport of 0.78 Sv with an rms error of 0.18 Sv. The transport time series exhibits significant intraseasonal variabilities, including variability on time scale close to the resonance period of the deep channel in the Luzon Strait (~30 days). Higher transports are connected with a higher velocity and a thicker overflow layer, allowing colder and saltier (thus denser) North Pacific Deep Water to flow into the South China Sea.

1. Introduction

The South China Sea (SCS), with an area of approximately 3.5×10^6 km^2 and a depth exceeding 4000 m in the central basin, is the largest marginal sea in the Southeast Asian Waters (Wyrtki, 1961). Connections between the SCS and the surrounding waters are mostly shallow: the Taiwan Strait to the East China Sea in the north, the Karimata Strait to the Java Sea in the south, and the Mindoro Strait to the Sulu Sea in the southeast. The 355 km wide Luzon Strait between the Taiwan and Luzon island (Fig. 1), with a sill depth of ~2400 m, is the only deep connection between the SCS and the surrounding waters. Through a deepwater overflow driven by the baroclinic pressure gradient between the Pacific Ocean and the SCS in the Luzon Strait, the North Pacific Deep Water (NPDW) spills into the SCS and generates a basin-scale cyclonic deep circulation (Qu et al., 2006a; Wang et al., 2011; Lan et al., 2013; Shu et al., 2014). The deep water in the SCS interior then upwells as a result of enhanced mixing (~10^{-3} m^2 s^{-1}, Tian et al., 2009), eventually exiting the SCS either in the intermediate layer through the Luzon Strait back to the Pacific Ocean (Chao et al., 1996; Chen and Huang, 1996; Qu et al., 2000; Tian et al., 2006; Zhang et al., 2015) or in the upper layer through shallow straits to the Java and Sulu Seas (Qu et al., 2009; Yaremchuk et al., 2009). This three-dimensional circulation constitutes a portion of the SCS throughflow and acts as a heat and freshwater conveyor that is believed to impact climate, both regionally and globally (Qu et al. 2006b).

A number of studies using different approaches have estimated the magnitude of the deepwater overflow through the Luzon Strait into the SCS (Tian and Qu, 2012). Indirect estimates on the basis of one-dimensional advective-diffusive heat balance (Wang, 1986) and hydraulic theory (Qu et al., 2006a) yielded a transport of 0.7 and 2.5 Sv, respectively; note the latter number represents the maximum hydraulically controlled transport through a rectangular channel narrower than the Rossby Radius (Whitehead, 1998). Later ship surveys of the current and hydrographic fields yielded estimates with a smaller range of 1 to 2 Sv (Tian et al., 2006; Yang et al., 2010; 2011). Based on repeated conductivity-temperature-depth (CTD) and lowered acoustic Doppler current profiler (LADCP) surveys, Zhao et al. (2014) yielded a transport of 1.4 Sv in the Luzon Strait and 1.1 Sv in the Bashi Channel. Direct estimates

* Correspondence to: Wei Zhao, 238 Songling Road, Physical Oceanography Laboratory/Qingdao Collaborative Innovation Center of Marine Science and Technology, Ocean University of China, Qingdao 266100, China.
E-mail address: weizhao@ouc.edu.cn (W. Zhao).

http://dx.doi.org/10.1016/j.dsr.2016.01.007
0967-0637/

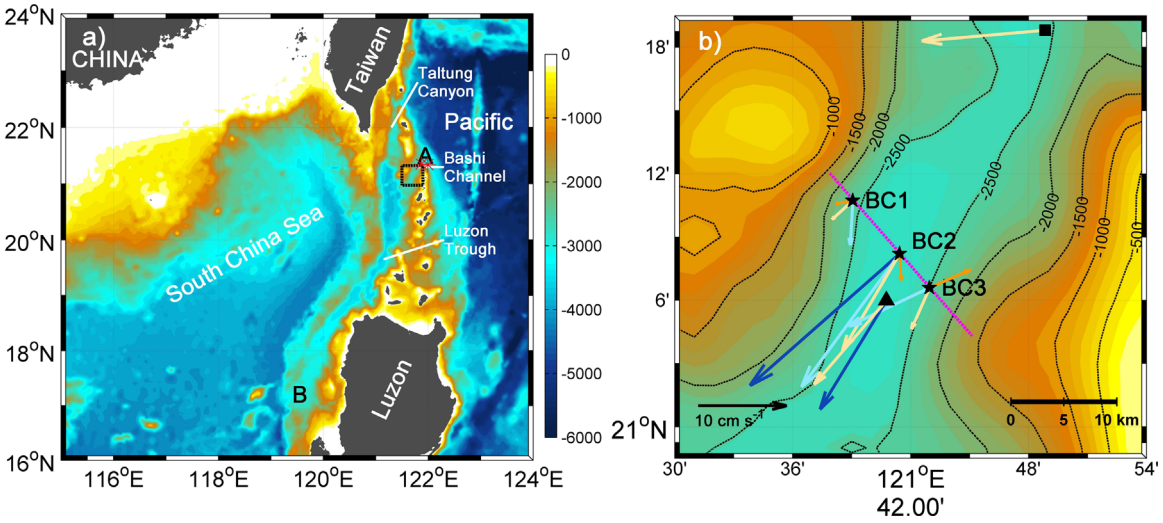

Fig. 1. Bottom topography in (a) the northeast part of the South China Sea and (b) the Bashi Channel based on version 15.1 of Smith and Sandwell (1997). Note the Luzon Trough extends approximately from 21°N to 17°N in the deep Luzon Strait. The red asterisks in (a) denote the locations of CTD profiles (used in Fig. 9). The black square, triangle, and stars in (b) denote the mooring locations in Liu and Liu (1988), Chang et al. (2010), and in this paper, respectively, with arrows representing the observed mean velocities. The pink dashed line indicates the section shown in Fig. 2. (For interpretation of the reference to color in this figure legend, the reader is reffered to the web version of this article.)

based on moored current meter data have also been made. Liu and Liu (1988) estimated a transport of ~1.2 Sv based on an 82-day current meter record in the Bashi Channel. Chang et al. (2010) estimated a similar mean transport value (1.06 Sv) from two nearly 10-month observation periods, which exhibit significant intraseasonal variations on time scales ranging from 30 to 60 days. The authors also deployed one mooring in the Taltung Canyon (the other channel in the Luzon Strait that is deeper than 2000 m, see Fig. 1) at the same time and found very weak mean flow there, confirming that the majority of the deep water enters the SCS through the Bashi Channel. More recently, Zhou et al. (2014) estimated a mean transport of 0.83 Sv in the Bashi Channel and 0.88 Sv further downstream in the Luzon Trough (which includes contribution from the Taltung Canyon) from a 3.5-year long mooring deployed at each location. Their transport time series also exhibited a significant seasonal variability (with a higher/lower transport in the late fall/spring, respectively), corresponding well with the seasonal variation of the density difference between the SCS and the Pacific Ocean close to the sill depth.

It is important to recognize that, although the transport values are generally comparable between Chang et al. (2010) and Zhou et al. (2014), there is one notable difference. With only a single mooring available, one has to make an inevitable assumption on the spatial, especially horizontal, structure of the flow. Chang et al. (2010) assumed a two-layer flow (separated by the mid-depth between the two instruments) that is homogenous horizontally across the channel, whereas Zhou et al. (2014) interpolated the velocity in cubic spline by assuming zero velocity at the two sidewalls. Although the channel is narrower than the Rossby Radius (~20 km), one wonders if the deepwater overflow exhibits a significant spatial structure that impacts the transport estimates. Also, although hydraulic theory has been previously used to estimate the upper limit of the transport (Qu et al., 2006a; Zhao et al., 2014), it remains unknown whether the flow is actually hydraulically controlled. To address these questions, two additional moorings were deployed in the Bashi Channel on both sides of the central mooring used by Zhou et al. (2014) from August 2010 to April 2011. Results from all three moorings are discussed in this paper. We found that.

a) The deepwater overflow exhibits a much stronger current in the middle than near the sides of the Bashi Channel. The isotherms, isohalines and isopycnals all bank upward to the right-hand side of the flow. The 8-month averaged transport is 0.78 Sv based on the three moorings (10 current meters) with an estimate of the total rms error of 0.18 Sv.
b) The Froude number at the Bashi Channel is much less than 1 and the signals propagate against the main stream of the overflow, both implying that the deep flow in the Bashi Channel could not be hydraulically controlled.
c) The overflow transport exhibits significant intraseasonal variabilities on a near 30 days time scale, which is close to the resonance period of the deep channel in the Luzon Strait. The higher transport is associated with a high velocity as well as an upward displacement of the upper interface of the overflow, allowing slightly colder, saltier (thus denser) NPDW to flow into the SCS.

2. Data

As part of the SCS deep circulation experiment, three bottom-anchored moorings were deployed in the Bashi Channel from August 2010 to April 2011 (see Fig. 1 for locations). 10 Aanderaa Instruments RCM Seaguard current meters and 7 SBE 37-SM CTDs were used to measure the current and hydrographic characteristics of the deepwater overflow (see Table 1 and Fig. 2 for the detailed instrument configurations). The instruments covered the entire depth below 2000 m, which is estimated to be the upper limit of the overflow based on the results from Zhao et al. (2014). With multiple deployments during a 3.5-year period, the central mooring BC2 collected significantly more data and the results have been discussed in Zhou et al. (2014). Only the data collected from August 2010 to April 2011 are used for the present study. All but one of the instruments (the CTD at 2406 m on BC2) returned high-quality data at hourly sampling intervals. As stated by the manufacturers, the measurement accuracies are: ~0.15 cm s^{-1} for velocity, 0.002 °C for temperature, 0.003 mS cm^{-1} for conductivity, and 0.1% of full scale range for pressure (or ~7 m for the CTDs). The vertical excursion of the instruments is relatively small as well

Table 1
Mooring configurations. Note the CTDs are 5 m deeper than the RCMs at each layer.

Mooring	Location	Depth (m)	Recording period	Instrument depth (m)
BC1	121°39.060′E 21°10.740′N	2397	08/17/2010–04/16/2011	2027(RCM+CTD) 2127 (RCM) 2277 (RCM+CTD)
BC2	121°41.436′E 21°08.218'N	2721	08/15/2010–04/16/2011	2001 (RCM+CTD) 2201 (RCM) 2401 (RCM+CTD) 2601 (RCM+CTD)
BC3	121°44.956′E 21°06.627′N	2500	08/17/2010–04/16/2011	1980 (RCM+CTD) 2180 (RCM) 2380 (RCM+CTD)

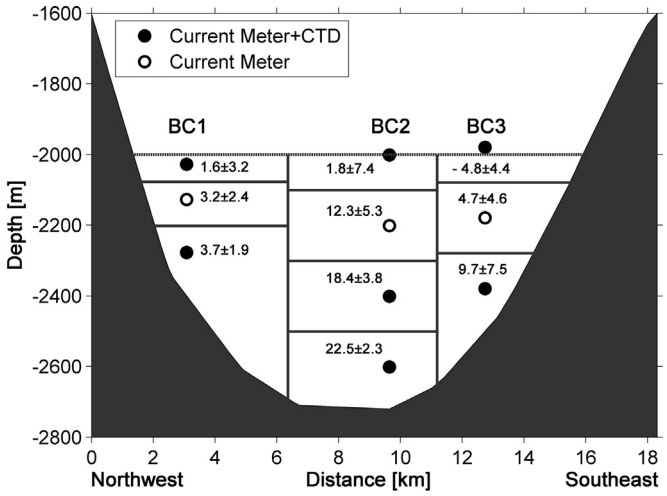

Fig. 2. Section view of topography from northwest to southeast and locations of the current meters and CTDs. The numbers are mean and standard deviations of the observed along-channel velocities (in cm s^{-1}).

(within 50 m for 96% of the observation period based on the pressure records) and thus, any errors resulting from vertical displacement of the instruments are negligible in this discussion.

Strong tidal signals are evident in the time series of zonal and meridional velocity, potential temperature, and salinity. Fig. 3 shows the original time series for the deepest instruments on the central mooring (BC2), where the strongest inflow of the coldest and most saline overflow water is observed. Using harmonic analysis we estimated the tidal amplitudes in both zonal and meridional directions for the four key tidal components: 15.3/11.7, 10.1/9.8, 6.8/9.2, and 7.1/5.1 cm s^{-1} for M2, K1, O1, and S2, respectively. Since we are specifically interested in sub-inertial flow, a 3-day Butterworth low-pass filter is applied to each of the time series to exclude the inertial (~33 h at the latitude of the Bashi Channel) and tidal effects. It should be noted that the diurnal components of K1 and O1 in the Luzon Strait interact and give rise to spring-neap tidal variability of approximately 14 days (e.g., Alford et al., 2011; Buijsman et al., 2012; Fang et al., 2015). This variability is also presented in the unfiltered hourly velocity time series.

3. Results

In this section we provide a (Section 3.1) general description of the overflow observed in the Bashi Channel, (Section 3.2) detailed discussion of its mean structure and volume transport including uncertainties, and (Section 3.3) follow-up discussion on its temporal variability and associated spatial structure.

3.1. General characteristics of the Bashi Channel deepwater overflow

We projected the observed horizontal velocity onto along-channel (V_a) and cross-channel (V_c) components, with the cross-channel direction defined as parallel to the section of moorings (pink dashed line in Fig. 1b). The orientation of the mooring section was based on results of the first 10-month deployment at the central mooring BC2: to be perpendicular to the direction (227°) of maximum mean velocity observed at 2600 m. The 3-day low-passed filtered time series of V_a, potential temperature θ, salinity S, and potential density referring to 2000 m (σ_2) at the three mooring locations are shown in Fig. 4, and the 8-month mean and standard deviation of V_a are illustrated in Fig. 2. The strongest V_a is observed near 2600 m on the central mooring, approximately 22.5 ± 2.3 cm s^{-1}. This mean and standard deviation values are comparable to 19.9 ± 6.5 cm s^{-1} in Zhou et al. (2014) based on the 3.5-year data. However, it is significantly stronger than 14.4 cm s^{-1} observed slightly downstream at 2695 m by Chang et al. (2010) (see Fig. 1b). The overflow water (at 2600 m on BC2) has an averaged potential temperature and salinity of 1.79 °C and 34.64 psu, respectively. The variations of temperature and salinity correlate with the variation of velocity (with a correlation coefficient of about 0.6, significant on 99% level): higher transport is associated with colder and saltier NPDW.

The time mean V_a decreases toward shallower depths and reaches only 1.8 cm s^{-1} at 2000 m. The variability of V_a, however, increases toward shallower depth. The standard deviation of the low-passed filtered current is 7.4 cm s^{-1} at 2000 m, compared to 2.3 cm s^{-1} at 2600 m. Strong current reversals can be found at 2000 m (Fig. 4b). This suggests that although 2000 m is a good approximation for the time mean upper limit of the overflow at this mooring location; the interface moves vertically as a function of time.

Much lower mean current velocity is seen at mooring locations BC1 and BC3 as compared to the central mooring BC2 (Fig. 2). The highest mean velocity at BC1 and BC3 is 3.7 and 9.7 cm s^{-1}, respectively, compared to 22.5 cm s^{-1} at BC2. At all three mooring locations, the variability of observed velocity is highly correlated between different depths, with their correlation coefficients higher than 0.77 (significant on 99.9% level). Horizontally, the variations of observed velocity at the same depth are also correlated (with a correlation coefficient of about 0.43 and significant on 95% level) between different moorings. Since the channel is relatively narrow, this is to be expected.

3.2. Mean section and volume transport

Fig. 5a shows the 8-month averaged V_a based on the 10 current meters affixed to the three moorings. The bottom topography is based on version 15.1 of Smith and Sandwell (1997) with 1-min resolution. The same topography is also used in Zhou et al. (2014) and an earlier version in Qu et al. (2006a). Without data from an echosounder survey along the section, it is difficult to assess the overall accuracy in this region. But the depths at the three mooring locations do compare well with that in the topography product. In constructing Fig. 5a, we assume zero velocity at the bottom and, for each mooring location, linearly interpolated V_a from the shallowest current meter (near 2000 m) to the bottom every 20 m. If the observed velocity at the shallowest current meter is positive (southwestward), V_a is further extrapolated linearly upward until a zero velocity is reached. Horizontally, V_a is interpolated every 200 m using cubic spline, with the assumptions of zero velocity at the two sidewalls.

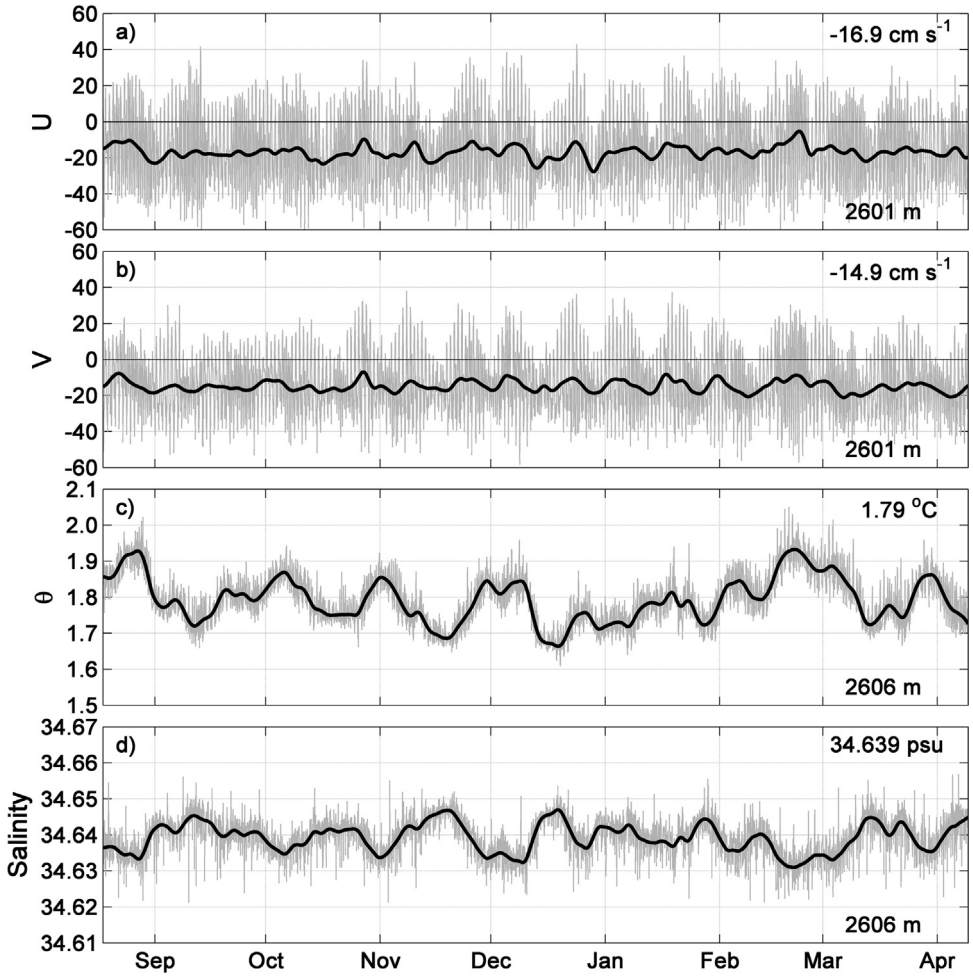

Fig. 3. Time series of observed (a) zonal velocity U (b) meridional velocity V, (c) potential temperature and (d) salinity near 2600 m at the central mooring BC2. The thin gray lines and thick black lines indicate the original hourly time series and 3-day low-passed filtered time series.

Fig. 5b–d shows the distributions of potential temperature θ, salinity S and potential density σ_2 based on data collected by the 6 CTDs (We chose not to extrapolate θ/S/σ_2 values in area beyond the coverage of observations). Due to the influence of Coriolis force, the isotherms, isohalines, and isopycnals all sloping upward to the right-hand side of the flow. We can estimate the baroclinic geostrophic current in the central part of the passage using the two density profiles from moorings BC1 and BC3. The vertically averaged geostrophic velocity over 2020–2280 m (with data coverage between BC1 and BC3) is 9.3 cm s^{-1}. This is close to the observed mean velocity of 8.9 cm s^{-1} on BC2 for the same depth range, suggesting that the current is approximately geostrophic.

The volume transport of the deepwater overflow can be estimated for every time step from the 3-day low-passed filtered velocity time series as shown in Fig. 3, using the same method as described in Fig. 5a. The 8-month transport time series is shown in Fig. 6a (thick black line). The mean and standard deviation of the transports are 0.78 and 0.35 Sv, respectively. Liu and Liu (1988) noted that it would require data from at least 10 current meters to calculate a reliable estimate of the transport in the Bashi Channel. Here we briefly examine the uncertainty of transport estimate with different numbers of current meters. Because the overflow is bottom intensified, a transport estimate based on one current meter measurement depends largely on the location of the current meter and can be quite unreliable. For example, using the maximum mean velocity of 22.6 cm s^{-1} (BC2 at 2600 m) and assuming a homogenous current below 2000 m, one can yield a transport estimate of 1.65 Sv, which is more than double the estimate indicated above. Using the central velocity profile from the BC2 mooring only, the uncertainty is largely due to the horizontal structure of the flow. A linear interpolation to zero velocity at the sidewalls results in a low transport limit of 0.57 Sv, while an assumption of homogenous velocity across the section gives rise to a high transport limit of 1.15 Sv (note the latter number is essentially the same as in Chang et al. (2010)). Using the central mooring only and a cubic spline interpolation as in Zhou et al. (2014) results in a transport of 0.82 ± 0.53 Sv for the 8-month mean (blue line in Fig. 6a). This mean transport value is similar to the 0.78 ± 0.35 Sv based on all 10 current meters on the three moorings (the standard deviation value is higher because of the higher variability on the central mooring; see Fig. 4). Another approach is to divide the section into 10 polygons based on the mooring configurations and the bathymetry between the two seamounts (Fig. 2). Assuming that velocity in each polygon is homogeneous, the cross-section transport of the overflow can be estimated. This estimate, 0.74 ± 0.33 Sv (red line in Fig. 6a), is similar to the value using the cubic spline interpolation (0.78 ± 0.35 Sv). Overall, the interpolation used in Zhou et al. (2014) based on one mooring fits well with the horizontal structure of the current at this location. Thus, it can be concluded that the 3.5-year mean transport estimate of 0.83 Sv given by Zhou et al. (2014) represents a reliable estimate for the long-term mean deepwater overflow through the Bashi Channel.

The additional mooring observations presented in this study, compared to Zhou et al. (2014), allow us to evaluate the

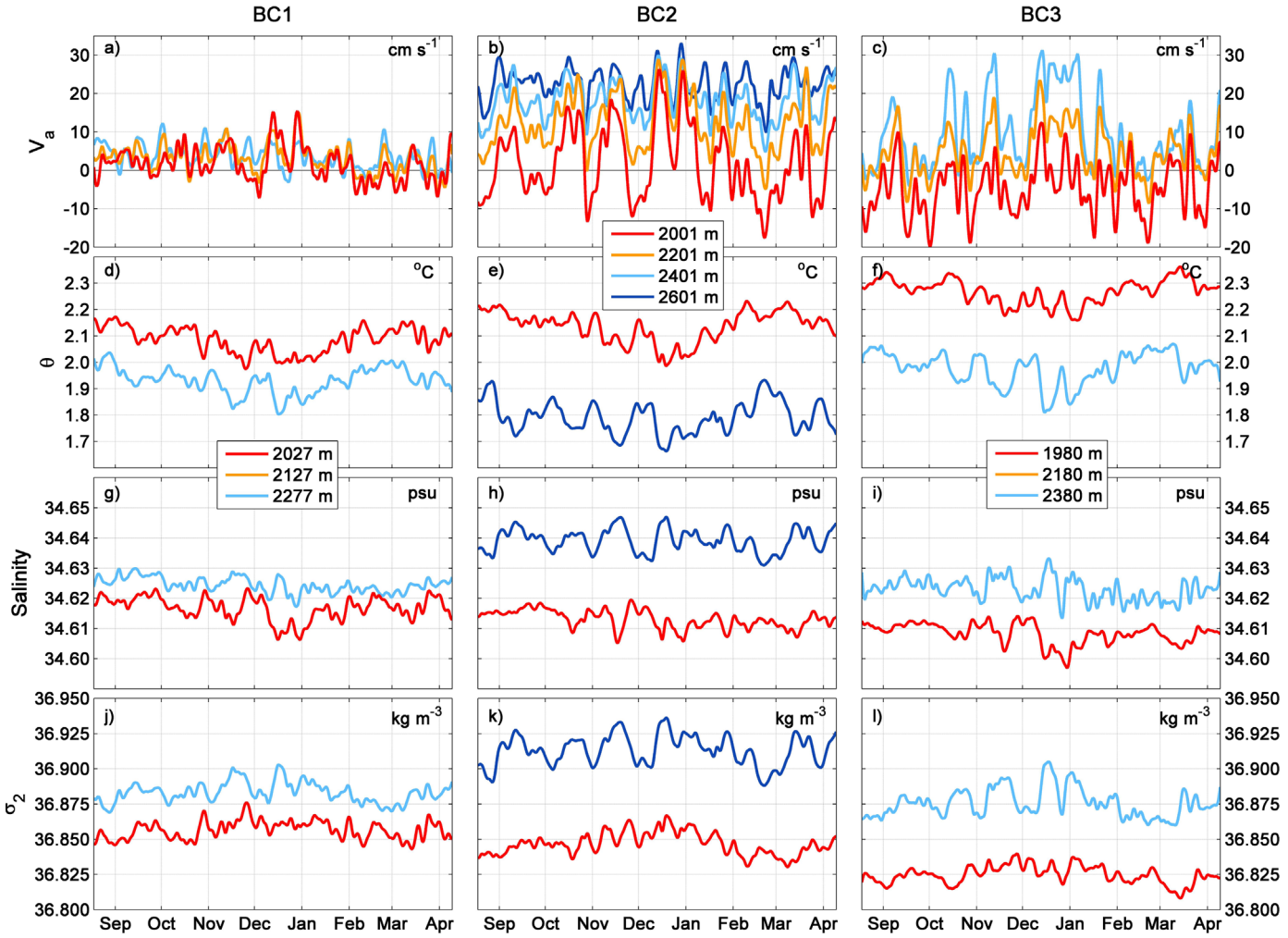

Fig. 4. The 3-day low-passed filtered time series of (a, b, c) along-channel velocity (in cm s^{-1}), (d, e, f) potential temperature (θ, in °C), (g, h, i) salinity (in psu) and (j, k, l) potential density (σ_2, in kg m^{-3}) at three moorings BC1, BC2 and BC3, respectively.

uncertainty of these assumptions regarding the spatial structure of the overflow and, for the first time, to obtain a transport error estimate at the Bashi Channel. A number of error sources are considered here:

a) Measurement error. The uncertainty in current measurement (0.15 cm s^{-1}) results in a small transport error of E_m=0.005 Sv.
b) The orientation of our mooring line. We calculated transport to be perpendicular to our mooring line. If we project observed velocity to a section perpendicular to the maximum mean flow at the central mooring, like in Zhou et al. (2014), the transport is 0.03 Sv higher. If we project the observed velocity to a section perpendicular to the topography contour, the transport is 0.06 Sv lower. So the uncertainty due to mooring configuration/location is E_c=0.06 Sv.
c) Vertical interpolation. We tried different interpolation schemes (linear, cubic spline, and logarithmic) from the deepest current meter to the bottom. The effect is: E_i=0.04 Sv.
d) We also calculated a standard error assuming a Gaussian distribution of the hourly transport values following Zenk et al. (1999). The essential degrees of freedom or number N of independent observations is calculated by the ratio of the record length T to twice the integral timescale τ. The latter was estimated from the integral of the normalized autocorrelation function of the transport time series from the origin to the first zero crossing: $N=T/(2\tau)=234.4\ \mathrm{d}/(2\times 8.4)\ \mathrm{d}\approx 14$. Further, the 95% confidence interval, E_T, due to the finite length of the time series can be calculated from the standard deviation, s:

$$E_T = s\frac{1.8}{\sqrt{N}} = 0.35\times\frac{1.8}{\sqrt{14}}\mathrm{Sv} = 0.17\mathrm{Sv}, \quad (1)$$

where the numerator comes from the Student t-test with 13 degrees of freedom (Table A.4 in Bendat and Piersol (2010)).

If we assume the known uncertainties to be independent, an estimate for the total rms error yields $E_T=\sqrt{E_m^2+E_c^2+E_i^2+E_T^2}$=0.18Sv associated with the mean transport of 0.78 Sv through the Bashi Channel (clearly the error comes mostly from E_T).

3.3. Temporal variability

The unfiltered transport time series based on 10 polygons (gray line in Fig. 6a) shows the high transport variability on diurnal scale. The signal of near 14 days spring-neap tidal cycle is also visible in Fig. 6a, more clearly in the zoomed panel Fig. 6b. The 3-day low-passed filtered time series of volume transport exhibits significant intraseasonal variabilities, ranging from 0.26 to 1.82 Sv for the 8-month period (Fig. 6a). Part of the variabilities are connected to the spring-neap tidal cycle. There are 16 spring tides and 17 neap tides during the observation period, and the averaged

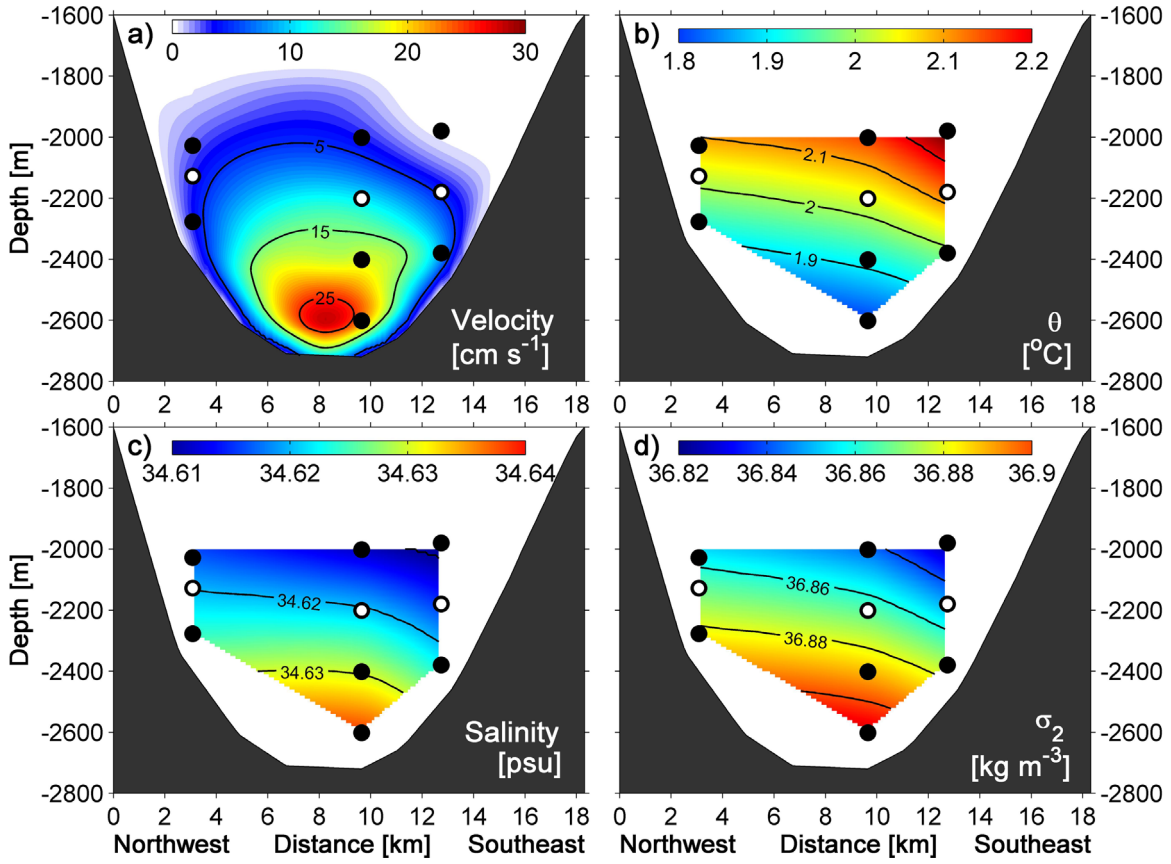

Fig. 5. Time-mean structures of (a) velocity (in cm s^{-1}), (b) potential temperature (in °C), (c) salinity (in psu), and (d) potential density (σ_2, in kg m^{-3}) in the Bashi Channel.

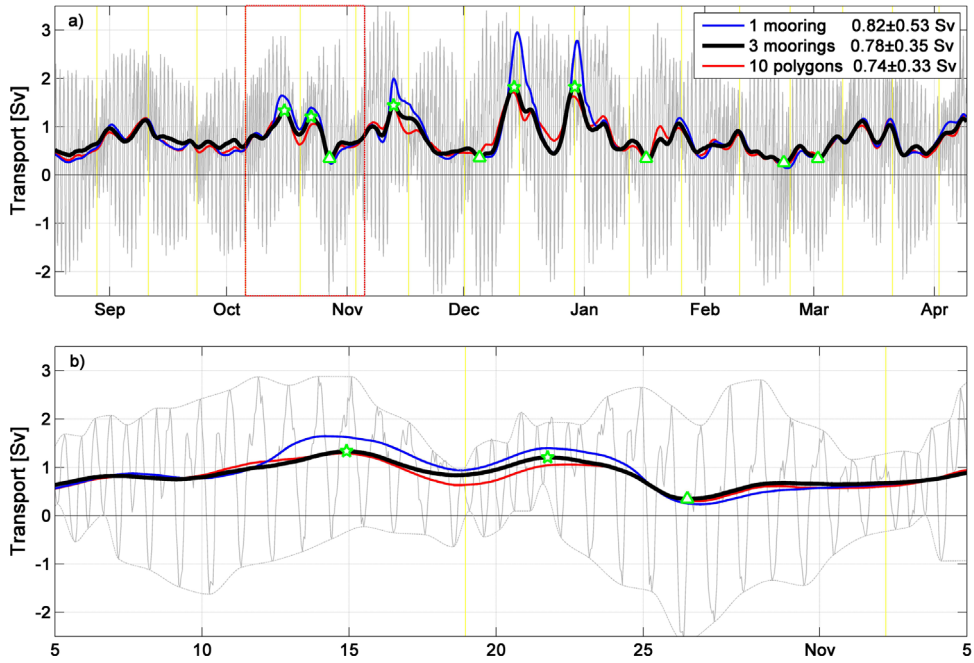

Fig. 6. Time series of the volume transport through the Bashi Channel over (a) the full 8-month observation period from August 2010 to April 2011 and (b) zoomed one month period from 5 October to 5 November (red box in a) estimated in different methods: The blue line is based on one mooring (BC2, 4 current meters); the thick black line is based on all three moorings interpolated with 10 current meters; the red line is based on 10 homogeneous velocity polygons (see Fig. 2); and the thin gray line is the unfiltered net transport time series based on 10 homogeneous velocity polygons. The vertical yellow lines indicated the neap times. Green stars and triangles denote events of highest and lowest transport using the cubic spline interpolation (thick black line), respectively, selected to illustrate the structure of the overflow in Figs. 8 and 9. The gray dashed lines in panel (b) indicate the high and low envelopes. (For interpretation of the reference to color in this figure legend, the reader is reffered to the web version of this article.)

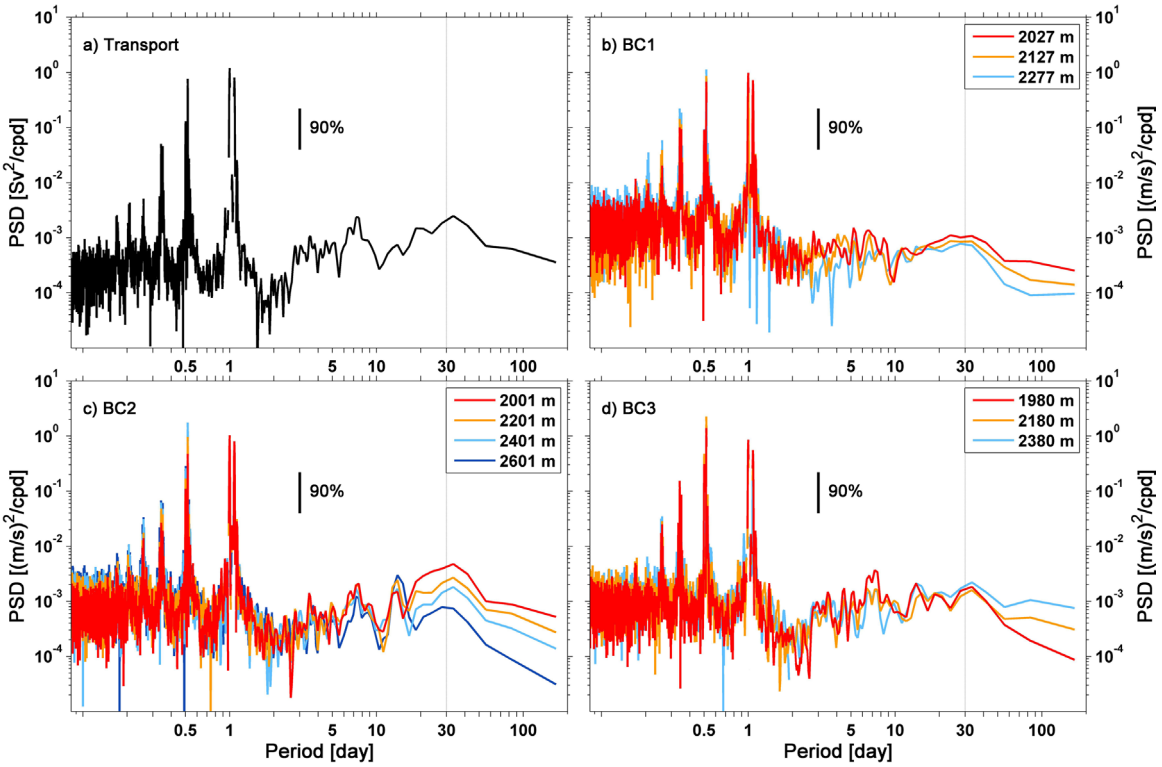

Fig. 7. Power spectrum density (PSD) of (a) the unfiltered net transport time series based on 10 homogeneous velocity polygons and (b, c, d) the along channel velocity at BC1, BC2, and BC3 moorings at each depth. Vertical bars indicate the 90% statistical significance level for the periods of 30 days.

overflow transport is about 0.70 Sv for the spring tides and 0.88 Sv for the neap tides, respectively. Thus, on average, the transport is weaker during spring tides than during neap tides, although the difference is smaller than the standard deviation of the transports for spring tides or neap tides ($\sim$0.30 Sv).

The transport also varies on a longer, $\sim$30 days time scale. This can be seen more clearly in the spectrum analysis of the transport based on 10 polygons (Fig. 7a) as well as the velocity time series (Fig. 7b–d). Zhou et al. (2014) found a similar 30 days variability at this location and $\sim$154 km downstream at the Luzon Trough in their 3.5-year time series, in addition to some longer term variability, and attributed this to deep eddies without substantial examination. Here we examine if intrinsic dynamics such as resonance could play a role in the 30 days variability mechanism. Resonance occurs at a specific frequency when a pipe's length equals one quarter of the wavelength in the case of the pipe with one end open and the other end closed; see Rudnick (1997) for an example in the deepwater overflow through the Samoan Passage in the Pacific Ocean. Here, we view the deep channel in the Luzon Strait as the "pipe", with the open end being the gate of the Bashi Channel (near 122.0°E, 21.5°N, as A in Fig. 1a) and the closed end being the southern end of the Luzon Trough (near 119.5°E, 17.0°N, as B in Fig. 1a). Given that the pipe's length is estimated to be 560 km, four times of this length (2240 km) would be the resonance wavelength of the throughflow. And we can obtain the resonance period, T, as the wavelength divided by shallow water wave phase speed c.

$$T = \frac{\lambda}{c} = \frac{\lambda}{\sqrt{g'h}}, \tag{2}$$

in which reduced gravity $g' = g\Delta\rho/\rho$ and h is the thickness of the abyssal layer. The average value of h is 1200 m, as estimated from four repeat-occupation stations in the Luzon Strait by Zhao et al. (2014; their Fig. 3a). $\Delta\rho$ is the density jump through the deep channel and taken to be 0.06 kg m^{-3} (Qu et al., 2006a). From these parameters, a phase speed c of 0.82 m s^{-1} can be derived, which produces a resonance period estimate of 31.4 days. This is in good agreement with the peak time scale (30 days) identified by spectrum analysis. The resonance offers a possible mechanism for the 30 days variability observed at this location. It is important to note that this is a very rough estimate, and other mechanisms may be important as well, for example the topographic Rossbywave (e.g., Thompson 1977; Johns and Watts 1986; Pickart and Watts 1990). A more comprehensive evaluation on this issue would require observations both upstream and downstream, which are unfortunately unavailable at this time.

Hydraulic theory has been widely used for prediction of overflow transport and variability in the deep passages (e.g., Whitehead, 1998; Girton et al., 2006; Qu et al., 2006a). Density profiles presented by Zhao et al. (2014) suggest that there is a large density difference between the SCS and the Pacific Ocean near 2000 m (which drives the overflow). Their velocity observations also show that the upper interface of the overflow is deeper in the Luzon Trough than in the Bashi Channel. These indicate that the NPDW in the SCS likely is deeper than that in the Pacific Ocean, a supportive scenario for hydraulically controlled flow. Here we follow the three criteria as introduced in Girton et al. (2006) to examine whether the overflow in the Bashi Channel is indeed hydraulically controlled:

a) Local Froude numbers: For a hydraulically controlled flow over sill, the Froude number $F=V/\sqrt{g'D}$ is expected to be <1 (subcritical) upstream, $=1$ at the critical section near the crest of the sill, and >1 (supercritical) downstream of the sill. At the mooring location BC2 (downstream of the sill), D is $\sim$900 m based on Fig. 5, g' is estimated $\sim 7.5\times10^{-4}$ m s^{-2} from the moored T/S, and V the vertical averaged deep current is 13.8 cm s^{-1}. These give $F=0.2$, which is much less than 1 and implies that the deep flow in the Bashi Channel could not be hydraulically controlled.

b) Parabolic channel. Assuming 1) the Bashi Channel has a parabolic cross section with the bottom elevation given by $h=h_0+\alpha x^2$, x being the distance in cross-channel direction, and 2) the potential vorticity $q=(f+\partial V/\partial x)/D$ of the flow is uniform, the Froude number can be expressed as

$$F_p^2=\frac{T^2(x_a+x_b)^2}{(w-2Tq^{-1/2})\left\{w-2Tq^{-1/2}+(T^2-1)[w-(1+2\alpha)T\alpha^{-1}q^{-1/2}]\right\}}, \quad (3)$$

where $T=\tanh(wf/\sqrt{g'D_\infty})$, $D_\infty=f/q$, $w=x_a-x_b$, and x_a and x_b denote the positions of the edges of the flow. At the Bashi Channel (Fig. 5), $\alpha=-17.5$, $f=5.3\times10^{-3}\ s^{-1}$, $\partial V/\partial x=\sim1.5\times10^{-4}\ s^{-1}$, $D=\sim900$ m, $x_a=0$, $x_b=18$ km. These give $F_q=0.1$, which is much less than 1 and suggests that the deep flow in the Bashi Channel could not be hydraulically controlled.

c) Wave speeds: We cannot calculate the wave speeds based on the available data at one section. However, Zhou et al. (2014) examined the 3.5-year long mooring observations in the Bashi Channel and further downstream in the Luzon Trough and found that the two time series are correlated most of the time (their Figure 10c). In spring and sometimes in October, when intraseasonal variations are intensified, the time series at the Luzon Trough leads that at the Bashi Channel by ~30 h. This implies that the signals propagate against the main stream of the overflow and the deep flow in the Bashi Channel could not be hydraulically controlled.

The results above consistently suggest that the deep overflow in the Bashi Channel is unlikely to be hydraulically controlled based on the data as much as we collected. And this may offer one explanation that the volume transport we estimated using cubic spline interpolation (0.78 Sv) is significantly lower than the upper transport limit (2.5 Sv) determined using hydraulic theory.

The good vertical and horizontal coverage of measurements allows us to assess if the observed transport variability is connected to spatial structure change. Five outliers with each sample in the data range of one day are out of the range of standard deviation (indicated in Fig. 6a) were selected and averaged to show

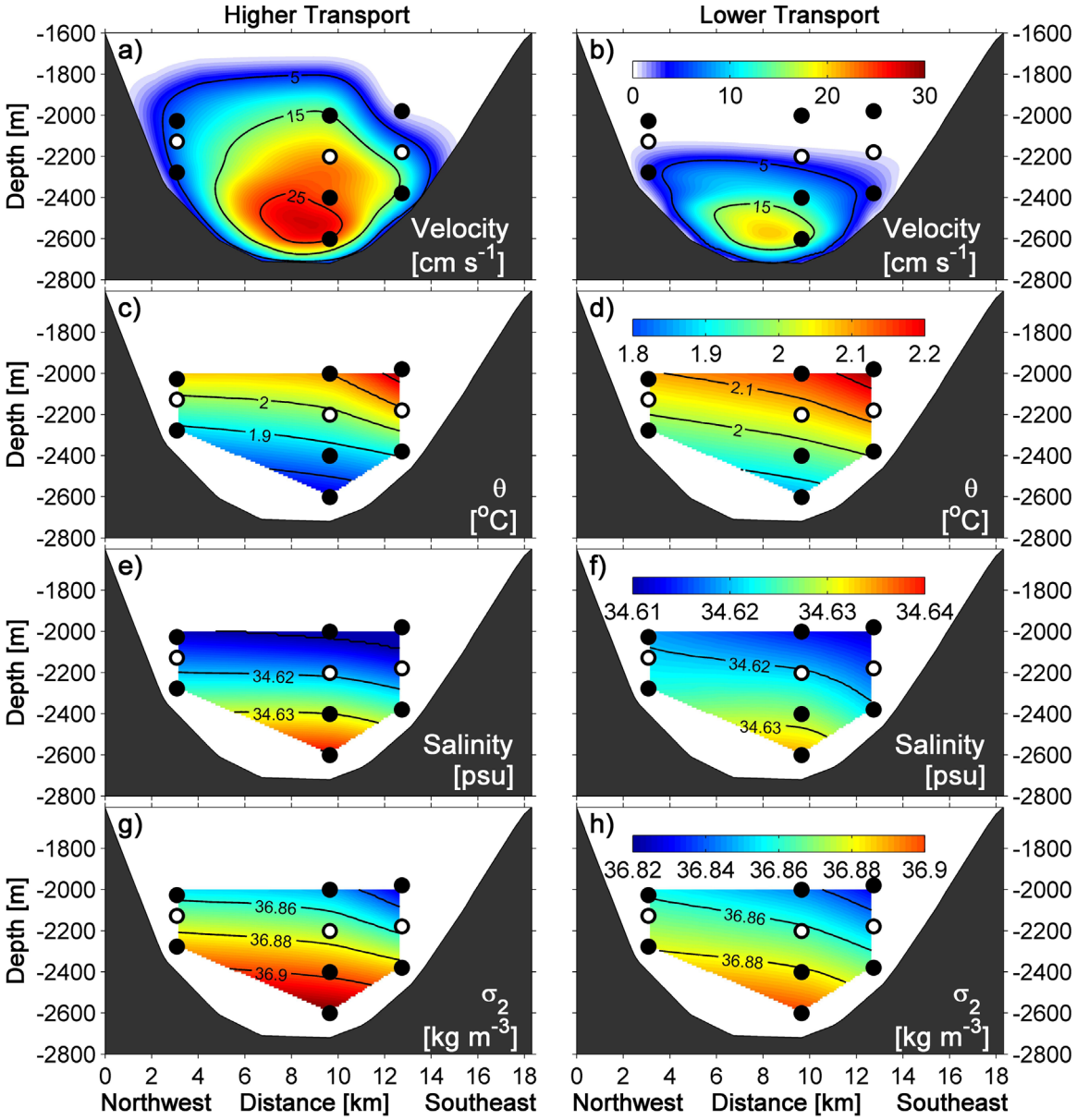

Fig. 8. Averaged spatial structures of (a, b) along-channel velocity (in cm s^{-1}), (c, d) potential temperature (in °C), (e, f) salinity (in psu) and (g, h) potential density (σ_2, in kg m^{-3}) corresponding to the five highest and lowest of transport scenarios as marked in Fig. 6 in the Bashi Channel.

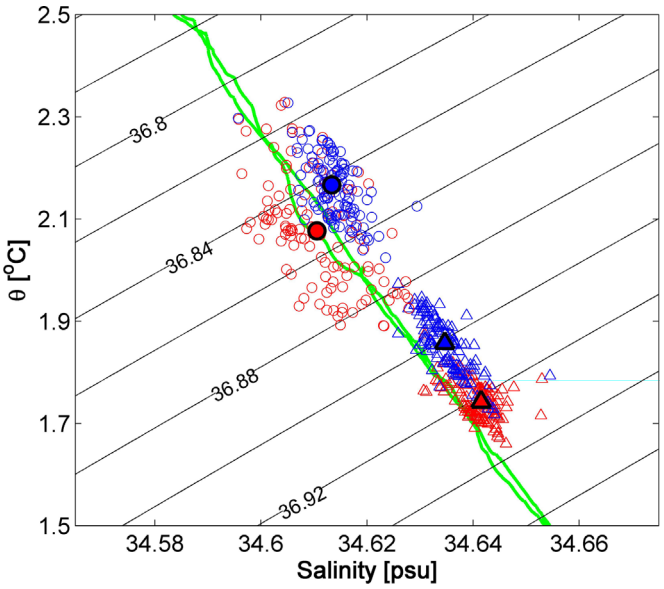

Fig. 9. Relation of potential temperature versus salinity (with σ_2 contours overlain) at 2000 m (circles) and 2600 m (triangles) of BC2 recorded by mooring CTDs and at the gate of the Bashi Channel by CTD profiles (green lines). Five highest (red) and lowest (blue) transport occasions marked in Fig. 6 were displayed with each sample in the data range of one day (120 circles/triangles for each case). Filled patterns represent averages. (For interpretation of the reference to color in this figure legend, the reader is reffered to the web version of this article.)

the spatial structure of velocity, potential temperature, salinity, and potential density in extreme scenarios (Fig. 8). The result indicates that higher transports are connected to higher velocities, thicker overflow layers, and colder and saltier (thus denser) NPDW in the Bashi Channel, and vice versa. Using two CTD profiles at the gate of the Bashi Channel during August 2008 (Fig. 1a), the relationship of potential temperature versus salinity at 2000 m and 2600 m of BC2 is illustrated in Fig. 9. The average potential temperature and potential density (σ_2) differences at 2600 m between higher and lower transports are $\sim$0.1 °C and $\sim$0.02 kg m^{-3}, respectively, corresponding to a vertical displacement of $\sim$150 m based on the vertical gradients of temperature ($\sim 6.7\times10^{-6}$ °C m^{-1}) and density ($\sim$1.3 kg m^{-4}) estimated from CTD profiles. Thus, the colder temperatures may be a result of upward isopycnal displacement in the Pacific Ocean, which allows denser/colder NPDW to enter the channel. This is consistent with the results shown in Fig. 8. As the deep water flows into the SCS through the Luzon Trough, the overflow water properties will be modified due to the diapycnal mixing with ambient water. Further observations along the flow pathway are needed to quantify the modification of the overflow water into the SCS.

4. Summary and discussion

The deepwater overflow through the Bashi Channel, as has been shown in the moored current meter measurements of Chang et al. (2010) and Zhou et al. (2014), is the main deepwater flow from the Pacific Ocean into the SCS. An accurate transport estimate of this overflow is critical to understanding the deepwater connection between the SCS and the surrounding water, and will lead to a better understanding of the deep circulation of the SCS. The two earlier studies mentioned in this paper yielded generally comparable transport estimates: 1.06 Sv in Chang et al. (2010) and 0.83 $\pm$ 0.46 Sv in Zhou et al. (2014). Both studies used measurements from a single mooring, and therefore the horizontal distribution of the overflow was not clear.

In this study, we used results from 10 current meters on three mooring locations to investigate the spatial structure, volume transport estimation, and temporal variability of the deepwater overflow through the Bashi Channel. The observed current is coherent both vertically and horizontally. Observations revealed substantial variation in the current, with a higher velocity in the middle than on the sides of the channel. The maximum velocity observed at 2600 m on the central mooring has a mean velocity of 22.5 $\pm$ 2.3 cm s^{-1}, a potential temperature (θ) of 1.79 $\pm$ 0.053 °C, a salinity of 34.64 $\pm$ 0.003 psu, and a potential density (σ_2) of 36.913 $\pm$ 0.009 kg m^{-3}, respectively. The current is approximately geostrophic, with the isotherms, isohalines and isopycnals all sloping upward to the right-hand side of the flow, corresponding to the bottom intensification of the current.

The 8-month mean transport of the overflow is estimated at 0.78 Sv, with a total rms error of 0.18 Sv, using cubic spline interpolation horizontally assuming zero velocity at the side walls. The low-passed filtered transport has a standard deviation of 0.35 Sv. It appears that, with only one mooring available, application of this assumption on the horizontal distribution of the current is well suited for narrow channels such as the Bashi Channel. However, assuming constant current across the channel or using linear interpolation to zero velocity at two sides of the channel will lead to over/under-estimated transports.

During the period of observation, the 3-day low-passed filtered volume transport varied from 0.26 to 1.82 Sv, with a maximum observed in December and a minimum in February. The transport (as well as the velocity) time series exhibit a 30 days variability. This time scale is close to the resonance period of the deep channel in the Luzon Strait. By averaging the five highest and lowest transport occasions, we showed that higher transports are connected to larger cross-section velocities and thicknesses, with colder, saltier, and denser NPDW entering the SCS through the Bashi Channel. The deepwater overflow in the Bashi Channel is unlikely to be hydraulically controlled as the Froude number is much smaller than 1. Without observations in the upstream of the Bashi Channel, we were unable to assess if similar variability takes place upstream in the Pacific Ocean. Further detailed observations in the region are needed to address the question of what drives the intraseasonal transport variability of the deepwater overflow.

Acknowledgment

This work was supported by National Key Basic Research Program of China (Program 973) (Grant no. 2014CB745003), the Foundation for Innovative Research Groups of the National Natural Science Foundation of China (Grant no. 41521091), the NSFC-Shandong Joint Fund for Marine Science Research Centers (Grant no. U1406401), Global Change and Air-Sea Interaction Project (Grant nos. GASI-03-01-01-03, GASI-IPOVAI-01-03), the National Natural Science Foundation of China (Grant nos. 41176010, 41576009), and the National High Technology Research and Development Program of China (Grant nos. 2013AA09A501, 2013AA09A502). In addition, the present paper benefited a lot form the helpful discussions with Tangdong Qu. We also thank two anonymous reviewers to provide several helpful comments for improving this paper.

References

Alford, M.H., MacKinnon, J.A., Nash, J.D., Simmons, H., Pickering, A., Klymak, J.M., Pinkel, R., Sun, O., Rainville, L., Musgrave, R., Beitzel, T., Fu, K.-H., Lu, C.-W., 2011. Energy flux and dissipation in Luzon Strait: two tales of two ridges. J. Phys. Oceanogr. 41, 2211–2222. http://dx.doi.org/10.1175/JPO-D-11-073.1.

Bendat, J.S., Piersol, A.G., 2010. Random Data: Analysis and Measurement Procedures, Fourth edition. Wiley, USA, p. 604.
Buijsman, M.C., Legg, S., Klymax, J.M., 2012. Double-ridge internal tide interference and its effect on dissipation in Luzon Strait. J. Phys. Oceanogr. 42, 1337–1356. http://dx.doi.org/10.1175/JPO-D-11-0210.1.
Chang, Y.-T., Hsu, W.-L., Tai, J.-H., Tang, T.-Y., Chang, M.-H., Chao, S.-Y., 2010. Cold deep water in the South China Sea. J. Oceanogr. 66, 183–190. http://dx.doi.org/10.1007/s10872-010-0016-x.
Chao, S.-Y., Shaw, P.T., Wu, S.Y., 1996. Deep water ventilation in the South China sea. Deep-Sea Res. I 43 (4), 445–466.
Chen, C.-T., Huang, M.H., 1996. A mid-depth front separating the South China Sea Water and the Philippine Sea Water. J. Oceanogr. 52, 17–25. http://dx.doi.org/10.1007/BF02236530.
Fang, Y., Hou, Y., Jing, Z., 2015. Seasonal characteristics of internal tides and their responses to background currents in the Luzon Strait. Acta Oceanogr. Sin. 34, 46–54. http://dx.doi.org/10.1007/s13131-015-0747-z.
Girton, J.B., Pratt, L.J., Sutherland, D.A., Price, J.F., 2006. Is the Faroe Bank Channel overflow hydraulically controlled? J. Phys. Oceanogr. 36, 2340–2349. http://dx.doi.org/10.1175/JPO2969.1.
Johns, W.E., Watts, D.R., 1986. Time scales and structure of topographic Rossby waves and meanders in the deep Gulf Stream. J. Mar. Res. 44, 267–290.
Lan, J., Zhang, N., Wang, Y., 2013. On the dynamics of the South China Sea deep circulation. J. Geophys. Res. Oceans 118, 1206–1210. http://dx.doi.org/10.1002/jgrc.20104.
Liu, C.-T., Liu, R.-J., 1988. The deep current in the Bashi Channel. Acta Oceanogr. Taiwan 20, 107–116.
Pickart, R.S., Watts, D.R., 1990. Deep western boundary current variability at Cape Hatteras. J. Mar. Res. 48, 765–791.
Qu, T., Mitsudera, H., Yamagata, T., 2000. Intrusion of the North Pacific waters in the South China Sea. J. Geophys. Res. 105, 6415–6424. http://dx.doi.org/10.1029/1999JC900323.
Qu, T., Girton, J.B., Whitehead, J.A., 2006a. Deepwater overflow through Luzon Strait. J. Geophys. Res. 111, C01002. http://dx.doi.org/10.1029/2005JC003139.
Qu, T., Du, Y., Sasaki, H., 2006b. South China Sea throughflow: a heat and freshwater conveyor. Geophys. Res. Lett. 33, L23617. http://dx.doi.org/10.1029/2006GL028350.
Qu, T., Song, T., Yamagata, T., 2009. An introduction to the South China Sea throughflow: its dynamics, variability, and implication for climate. Dyn. Atmos. Oceans 47, 3–14. http://dx.doi.org/10.1016/j.dynatmoce.2008.05.001.
Rudnick, D., 1997. Direct velocity measurements in the Samoan Passage. J. Geophys. Res. 102, 3293–3302. http://dx.doi.org/10.1029/96JC03286.
Shu, Y., Xue, H., Wang, D., Chai, F., Xie, Q., Yao, J., Xiao, J., 2014. Meridional overturning circulation in the South China Sea envisioned from the high-resolution global reanalysis data GLBa0.08. J. Geophys. Res. Oceans 119, 3012–3028. http://dx.doi.org/10.1002/2013JC009583.
Smith, W.H.F., Sandwell, D.T., 1997. Global seafloor topography from satellite altimetry and ship depth soundings. Science 277, 1956–1962. http://dx.doi.org/10.1126/science.277.5334.1956.
Thompson, R.O.R.Y., 1977. Observations of Rossby waves near Site D. Prog. Oceanogr. 7, 1–28.
Tian, J., Yang, Q., Liang, X., Xie, L., Hu, D., Wang, F., Qu, T., 2006. Observation of Luzon Strait transport. Geophys. Res. Lett. 33, L19607. http://dx.doi.org/10.1029/2006GL026272.
Tian, J.W., Yang, Q.X., Zhao, W., 2009. Enhanced diapycnal mixing in the South China Sea. J. Phys. Oceanogr. 39, 3191–3203. http://dx.doi.org/10.1175/2009JPO3899.1.
Tian, J., Qu, T., 2012. Advances in research on the deep South China Sea circulation. Chin. Sci. Bull. 57, 3115–3120. http://dx.doi.org/10.1007/s11434-012-5269-x.
Wang, J., 1986. Observation of abyssal flows in the Northern South China Sea. Acta Oceanogr. Taiwan 16, 36–45.
Wang, G., Xie, S.-P., Qu, T., Huang, R.X., 2011. Deep South China Sea circulation. Geophys. Res. Lett. 38, L05601. http://dx.doi.org/10.1029/2010GL046626.
Whitehead, J.A., 1998. Topographic control of oceanic flows in deep passages and straits. Rev. of Geophys 36, 423–440. http://dx.doi.org/10.1029/98RG01014.
Wyrtki, K., 1961. Physical oceanography of the southeast Asian Waters Naga Rep. 2, p. 195. Scripps Inst. of Oceanogr. San Diego, Calif.
Yang, Q., Tian, J., Zhao, W., 2010. Observation of Luzon Strait transport in summer 2007. Deep-Sea Res. I 57, 670–676. http://dx.doi.org/10.1016/j.dsr.2010.02.004.
Yang, Q., Tian, J., Zhao, W., 2011. Observation of material fluxes through the Luzon Strait. Chin. J. Oceanol. Limnol. 29, 26–32. http://dx.doi.org/10.1007/s00343-011-9952-6.
Yaremchuk, M., McCreary Jr., J., Yu, Z., Furue, R., 2009. The South China Sea throughflow retrieved from climatological data. J. Phys. Oceanogr. 39, 753–767. http://dx.doi.org/10.1175/2008JPO3955.1.
Zhao, W., Zhou, C., Tian, J., Yang, Q., Wang, B., Xie, L., Qu, T., 2014. Deep water circulation in the Luzon Strait. J. Geophys. Res. 119, 790–804. http://dx.doi.org/10.1002/2013JC009587.
Zhang, Z., Zhao, W., Tian, J., Yang, Q., Qu, T., 2015. Spatial structure and temporal variability of the zonal flow in the Luzon Strait. J. Geophys. Res. 120, 759–776. http://dx.doi.org/10.1002/2014JC010308.
Zhou, C., Zhao, W., Tian, J., Yang, Q., Qu, T., 2014. Variability of the deep-water overflow in the Luzon Strait. J. Phys. Oceanogr. 44, 2972–2986. http://dx.doi.org/10.1175/JPO-D-14-0113.1.
Zenk, W., Siedler, G., Lenz, B., Hogg, N.G., 1999. Antarctic bottom water flow through the Hunter Channel. J. Phys. Oceanogr. 29, 2785–2801. http://dx.doi.org/10.1175/1520-0485(1999)029 < 2785:abwftt > 2.0.co;2.